Deep Learning-Aided OFDM Demodulation Scheme for Undersea RF Short-Range Communication

Idnin PASYA[1], Megat Syahirul Amin MEGAT ALI[2], Azrul Amri JAMAL[3]

[1] Dept. of Computer Science and Engineering, University of Aizu, 965-8580 Aizuwakamatsu, Fukushima, Japan
[2] Microwave Research Institute, Universiti Teknologi MARA, 40450 Shah Alam, Selangor, Malaysia
[3] Faculty of Informatics & Computing, Universiti Sultan Zainal Abidin, 22200 Besut, Terengganu, Malaysia

idnin@u-aizu.ac.jp, megatsyahirul@uitm.edu.my, azrulamri@unisza.edu.my

Submitted April 7, 2025 / Accepted October 13, 2025 / Online first December 12, 2025

Abstract. *The realization of undersea wireless communication using radio frequency (RF) signals is hindered by severe attenuation and signal distortion, particularly due to complex propagation mechanisms and limitations of RF hardware. This paper proposes a deep learning-based orthogonal frequency division multiplexing (OFDM) demodulation scheme that employs a long short-term memory (LSTM) network, thereby eliminating the need for conventional channel estimation and equalization. The proposed method is evaluated under two numerically modeled undersea RF channel scenarios: (i) direct-path propagation and (ii) combined direct and lateral wave propagation. While achieving performance comparable to conventional least squares (LS) demodulation for BPSK, QPSK, and 8-PSK in the direct-path case, the LSTM-based approach significantly outperforms the LS method under combined direct and lateral wave conditions, yielding a 2–6 dB improvement in bit error rate (BER) across various modulation schemes. Notably, the gain is more pronounced with higher-order modulations such as 8-PSK, demonstrating the potential of deep learning to enhance the robustness of undersea RF communication in challenging environments.*

Keywords

Undersea communication, OFDM, deep learning, long short-term memory (LSTM)

1. Introduction

A reliable communication link is essential in undersea applications such as environmental monitoring, search and rescue operations, and resource exploration. Since wired connections have physical limitations, wireless data transmission is desirable in many cases. Conventionally, wireless undersea communication systems are predominantly implemented using acoustic systems. However, these systems have a limitation in signal bandwidth, capping the achievable data rate. The utilization of radio frequency (RF) signals for undersea wireless communication enables the use of wider signal bandwidth, thereby increasing channel capacity. This presents a promising prospect for high-performance undersea wireless short-range communication, which benefits applications such as high-definition video streaming. Nevertheless, transmission of the RF signal in the undersea suffers from severe signal attenuation, especially at higher frequencies [1]. In addition, several challenges remain, including inefficient study of undersea RF propagation characteristics and a lack of models emulating signal impairments due to the noise of RF devices operating undersea. These factors hindered the realization of high-performance undersea RF transmission schemes, leading to ambiguous measurements and disagreement between simulated and measured results in some studies [2–4].

Under these critical circumstances, this work proposes replacing the traditional block-based signal processing method in undersea RF systems with a deep learning (DL)-based demodulation scheme. The motivation behind this approach is to leverage the power of deep neural networks in learning and compensating for the above-mentioned factors in undersea RF transmission systems. Recently, due to rapid advancements in deep neural networks, the use of DL methods in the physical layer of wireless communication has received significant attention. Typical examples of such work include the implementation of deep learning to partially replace the signal processing algorithms in 5G and future 6G systems [5], [6], as well as the implementation of black box models that replace both the transmitter and receiver with autoencoders [7]. The majority of research works focus on the former case; for example, DL-based networks are used for resource allocation and management [8], beam optimization [9], channel estimation [10–12], automatic modulation classification [13], and joint channel estimation and symbol detection [14]. One notable contribution in the regime of DL-based demodulation is DeepRx by Honkala et al. [5], which introduced a fully convolutional end-to-end receiver trained to directly recover transmitted bits from raw orthogonal frequency division multiplexing (OFDM) signals. Instead of relying on explicit synchronization, channel estimation, and symbol demapping, DeepRx replaces these modules with a data-driven neural network that implicitly learns to perform the corresponding tasks. While it performs well under terrestrial multipath fading, DeepRx operates on entire OFDM frames and lacks subcarrier- level modularity,

DOI: 10.13164/re.2025.0725

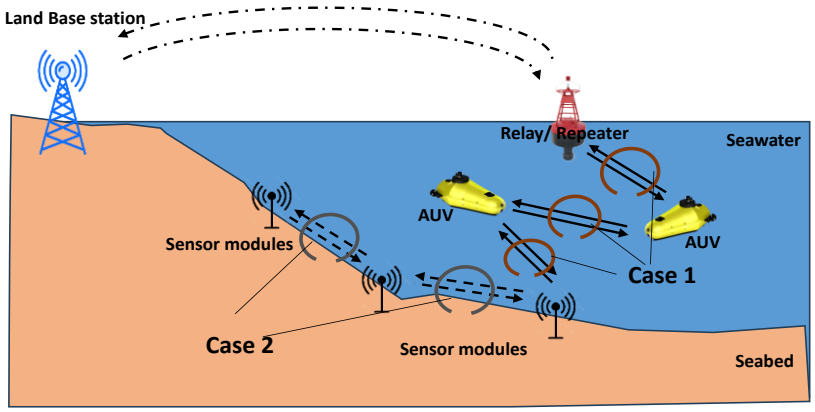

Fig. 1. Scenario of communication links in an undersea RF wireless communication network considered in this study.

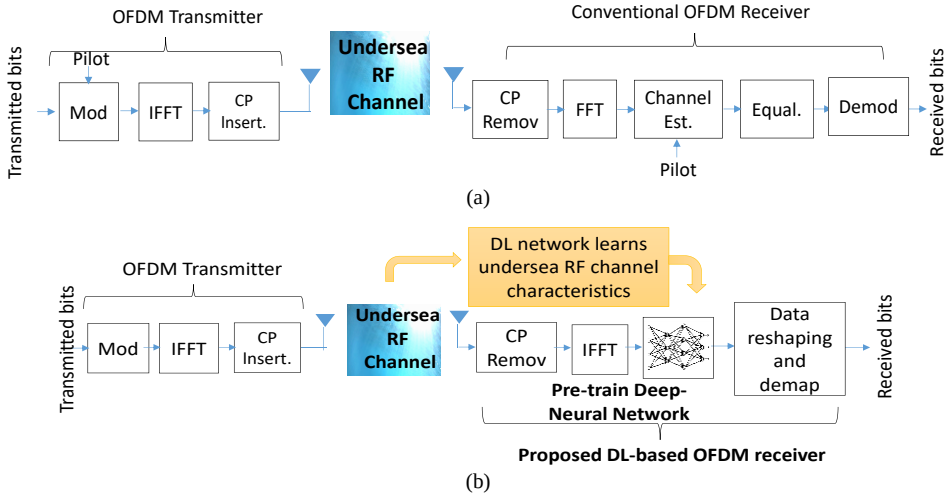

Fig. 2. Comparison of the proposed DL-based OFDM scheme with conventional OFDM receiver: (a) Conventional, (b) Proposed. [30]

which limits its flexibility and efficiency for resource-constrained platforms.

Several other deep learning-based OFDM demodulation schemes have been proposed. Siriwanitpong et al. [15] developed a one-dimensional convolutional neural network (1D-CNN)-based demodulator for high-speed railway environments, demonstrating low latency in the presence of rapid Doppler shifts. Rahman et al. [16] introduced a hybrid CNN-bidirectional long short-term memory (biLSTM) architecture that combines spatial and temporal feature extraction for joint detection in 5G non-orthogonal multiple access (NOMA)-OFDM systems. These models process full OFDM frames and require reshaping of the input to 2D formats, which increases complexity and may reduce flexibility.

More recently, ResNet-based architectures have been adopted for demodulation. Zhang et al. [17] employed a deep residual network to jointly perform channel estimation and signal detection in underwater acoustic OFDM systems. This deep architecture improves feature learning through skip connections, but is computationally expensive and requires large memory footprints. Li et al. [18] proposed TransDetector, a transformer-based detector for underwater acoustic differential OFDM communications, achieving notable BER gains through multi-head self-attention and denoising. However, these networks are not tailored to the unique properties of undersea RF channels, such as lateral wave propagation and static fading.

To the best of our knowledge, investigation into DL demodulation in undersea RF systems is absent from the literature. In this article, we propose a DL network in an undersea RF OFDM scheme, for joint channel estimation and symbol demodulation, to realize a more robust performance in the undersea RF channel. The DL network is used to initially learn the characteristics of the undersea channel affecting the received OFDM symbols and later utilized to demodulate the OFDM symbols without knowledge of channel state information (CSI) obtained through pilot symbols and equalization (Figs. 2 and 3). We consider an undersea wireless sensor network comprised of underwater sensor modules, autonomous underwater vehicles (AUV) and data relay/repeater unit is considered, as depicted in Fig. 1. In this stage of investigation, this study considers two representative cases of data transmission: (1) Case 1 – communication between sensors, AUV and data relay/repeater unit, (2) Case 2 – communication between sensor modules positioned near the seabed. The details of each case are explained in the following Sec. 2.

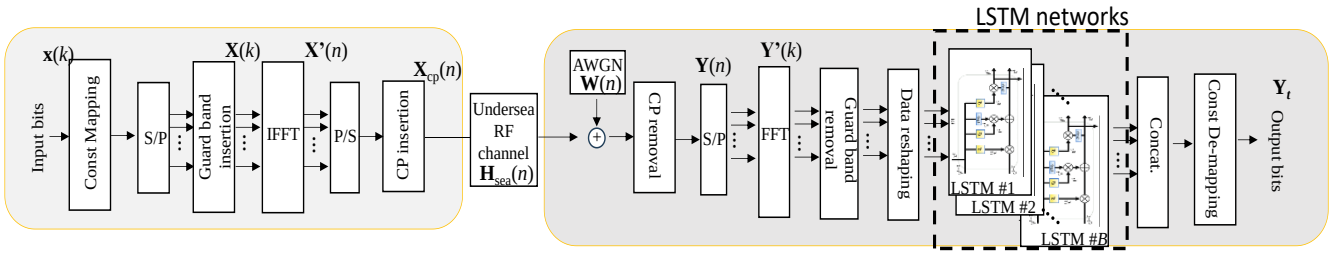

Fig. 3. Block diagram of the proposed DL-based OFDM scheme used in this study.

Method	DL Architecture	Target Domain	Input Format	Demodulation type	Training Granularity	Remarks
Honkala et al. [5]	Fully convolutional DL receiver	Terrestrial RF (5G)	Raw IQ samples	End-to-end bit recovery	Entire OFDM frame	Replaces complete Rx chain; Lacks subcarrier level granularity
Siriwanitpong et al. [15]	1D-CNN	High-speed railway network	1D time domain sequence	Frame-wise classifier	Entire OFDM frame	Simple and fast; No temporal modeling
Rahman et al. [16]	CNN + biLSTM	5G/NOMA uplink	2D reshaped OFDM frame	Joint estimation and detection	Entire OFDM frame	Combine spatial and temporal features; High computational burden
Zhang et al. [17]	ResNet	Underwater acoustic	Spectrogram	Joint estimation and detection	Entire OFDM frame	Tailored for acoustic channels; High complexity
Li et al. [18]	Transformer network with self-attention	Underwater acoustic	Time domain OFDM sequence	Differential OFDM symbol detection	Entire OFDM frame	Tailored for multipath-rich acoustic channels; High complexity
This work (proposed)	Subcarrier-wise LSTM	Undersea RF (short-range)	1D OFDM subcarrier stream	Symbol-level demodulation	Per subcarrier (modular)	Modular and parallelizable inference, faster convergence, and lower training complexity per subcarrier, Enables adaptive retraining; Aggregate overhead increases with the number of subcarriers

Tab. 1. Comparison with state-of-the-art DL-based OFDM demodulators.

The proposed DL-based undersea RF system is evaluated over an OFDM transmission scheme due to its spectrum efficiency, robustness, and scalability. Unlike the reports in [15] and [16] that used DNN and CNN as the learning network, this study implements a long short-term memory (LSTM) network at the OFDM receiver. This approach exploits the temporal dependencies in the received OFDM symbols to achieve robust demodulation at the subcarrier level. In addition, unlike CNN, LSTM networks do not require conversion of the bit stream into 2-dimensional matrices for the convolutional layer.

In this proposed scheme, an LSTM network is trained at each data subcarrier, where it is embedded with known OFDM symbols (training data) and the corresponding output (labels) for that subcarrier. The fully trained LSTM network processes and predicts the output at the subcarrier, and the overall received OFDM symbols are obtained by concatenating the predicted symbols from each data subcarrier.

The core novelty of the proposed scheme lies in its subcarrier-wise training strategy, where an individually trained LSTM network handles each data subcarrier. This modular design enables scalable and parallelizable deployment, which aligns well with multi-core architectures in embedded processors, where computational load can be distributed. Additionally, subcarrier-specific models reduce input dimensionality and learning complexity, allowing faster convergence and improved training efficiency. A specific subcarrier can also be selectively fine-tuned in response to evolving channel conditions, without retraining the entire system. This LSTM architecture also inherently captures the temporal dynamics of the received signal, which are significant in underwater RF channels represented in Fig. 1. A summary of the key differences between the proposed model and existing DL-based demodulators is provided in Tab. 1.

The authors have previously investigated the potential of the proposed LSTM network [19], where the effects of training data parameters on the demodulation performance were evaluated at one OFDM subcarrier. In this paper, we present a comprehensive analysis of the proposed scheme's performance, considering all data subcarriers, and assess the practical computational cost using representative embedded processing platforms. The contribution of this present paper is listed as follows:

1. Focus on the implementation of a DL-based demodulation for OFDM systems operating in undersea RF channels, evaluating the capability of the network to learn the

channel characteristics, and perform demodulation instead of conventional channel estimation and equalization. Performance is assessed in practical RF signal transmission conditions in an underwater wireless sensor network.

2. Present the implementation framework of the proposed DL-based undersea RF OFDM system, particularly describing the method to train the network separately on each of the OFDM subcarriers. This modular architecture naturally enables parallel processing, improved training efficiency per subcarrier, and allows adaptive retraining.

3. Based on the analysis of the numerical simulations, the proposed scheme outperforms the conventional channel equalization using the least squares (LS) method. It is also shown that the proposed scheme offers greater performance improvement in the case of higher-order subcarrier modulation.

4. The performance of the proposed scheme is evaluated and benchmarked with conventional demodulation schemes and similar DL-based demodulation in terms of performance and complexity.

The remainder of this paper is organized as follows. Section 2 describes the proposed DL-based undersea RF OFDM scheme model, a detailed description of the considered undersea RF channel model, network architecture, and training methods. Results and analysis are presented in Sec. 3, and Section 4 provides the concluding remarks and future works.

2. The Proposed Deep Learning-based OFDM Demodulation

2.1 Traditional OFDM Receiver and Frame Structure

The parameters of the base OFDM scheme used in this study are summarized in Tab. 2. Each OFDM symbol consists of $N = 64$ subcarriers, including 48 data subcarriers, and 16 null subcarriers (as guard bands). A cyclic prefix (CP) of either CP = 2 or 16 samples is appended, corresponding to 1/32 or 1/4 of the useful symbol duration, respectively. With a system sampling rate of 2 MHz and a subcarrier spacing of 31.65 kHz, the useful OFDM symbol duration, T_{symbol}, is approximately 31.6 µs, and the CP durations, T_{CP}, correspond to 1 µs and 8 µs, respectively.

We consider a transmission frame consisting of a total of L OFDM symbols, as illustrated in Fig. 4. The index of the OFDM symbol within the frame is denoted as l, where $l = 0, 1, \ldots, L-1$. Pilots are inserted using the block-type method, where odd-indexed symbols ($l = 1, 3, 5, \ldots$) are designated as pilot symbols, and all 48 active subcarriers in those symbols carry known pilot values. The even-indexed symbols ($l = 0, 2, 4, \ldots$) are used as data symbols. This arrangement enables robust channel estimation at the receiver. In this study, we assume perfect synchronization at the receiver to isolate and evaluate the demodulation performance of the proposed scheme.

Parameters	Value
Center frequency, f_c	1 MHz
No. of subcarriers, N	64
Subcarrier spacing	31.65 kHz
No. of data subcarriers, B	48
Number of null subcarriers	16
Cyclic prefix (CP)	Maximum 16 (1)
Symbol modulation	BPSK, QPSK, 8-PSK
Symbol mapping	Gray coded

(1) CP = 16 correspond to 1/4 of the OFDM symbol duration.

Tab. 2. Main parameters of the base OFDM scheme.

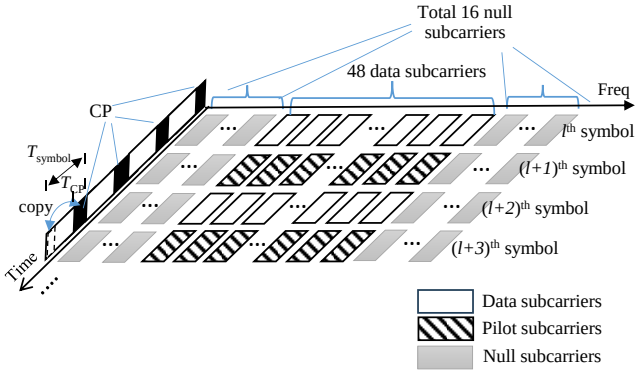

Fig. 4. Illustration of the base OFDM frame: the time axis shows alternating data and pilot symbols, the frequency axis shows the allocation of data, pilot, and null subcarriers, and the CP is appended in the time domain before each OFDM symbol.

Channel estimation is carried out in the frequency domain using the Least Squares (LS) estimator [20] on the pilot symbols

$$\hat{H} = \frac{Y(k)}{X(k)} \tag{1}$$

where $Y(k)$ and $X(k)$ are the received and known pilot values, respectively. Equalization is then performed using the Zero-Forcing (ZF) algorithm [20], where each received subcarrier is divided by the estimated channel response before symbol demapping.

2.2 Proposed Deep Learning-based OFDM Scheme

The baseline OFDM receiver structure, including CP and pilot arrangements, is described in Sec. 2.1. In this section, we developed the proposed DL-based demodulator that builds on this system. The schematic of the proposed scheme is depicted in Fig. 3. A series of binary data sequences is initially modulated with an M-ary modulation scheme using phase shift keying (PSK). In this study, gray-coded binary phase shift keying (BPSK), quadrature phase shift keying (QPSK), and 8-phase shift keying (8-PSK) are considered for analysis. The modulated signal is converted from serial to parallel, and pilot symbols are inserted for implementation of channel estimation, in the case of conventional demodulation

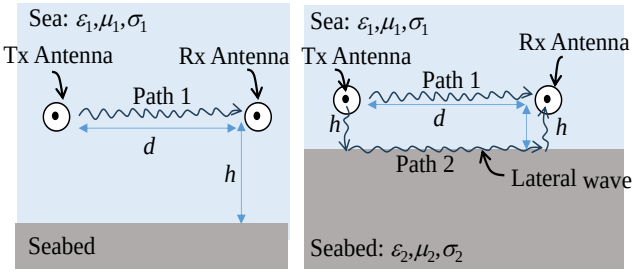

(a) (b)

Fig. 5. Undersea RF transmission modes under consideration (Reproduced from [19]): (a) Case 1 and (b) Case 2 (Near seabed).

methods, for benchmarking purposes. For the sake of simplicity, the utilization of coding techniques such as turbo and convolutional codes for forward error correction (FEC) is not considered at this stage of the investigation. Important parameters for the OFDM scheme are listed in Tab. 2. The time-domain signal $\mathbf{X}'(n)$ is obtained by conducting N-point IFFT over all of the subcarriers. We define this operation as

$$\begin{aligned}\mathbf{X}'(n) &= \mathrm{IFFT}\left[\mathbf{X}'(k)\right] \\ &= \sum_{k=0}^{N-1}\mathbf{X}'(n)\mathrm{e}^{\frac{\mathrm{j}2kn}{N}},\ n=0,1,2,\ldots,N-1\end{aligned} \tag{2}$$

where $\mathbf{X}'(k)$ is the transmitted frequency-domain OFDM symbol. A cyclic prefix (CP) of duration T_{CP} is appended to each OFDM symbol by copying the last T_{CP} samples of the symbol and placing them at its beginning, to form the transmitting signal denoted as $\mathbf{X}_{\mathrm{CP}}(n)$.

Next, $\mathbf{X}_{\mathrm{CP}}(n)$ is passed through an undersea RF communication channel with channel impulse response matrix $\mathbf{H}_{\mathrm{sea}}$. The signal entering the OFDM receiver is then modeled using standard baseband representation with additive white Gaussian noise (AWGN) [20], given by

$$\mathbf{Y}_{\mathrm{CP}}(n) = \mathbf{H}_{\mathrm{sea}}(n) * \mathbf{X}_{\mathrm{CP}}(n)\mathrm{e}^{\mathrm{j}2f_{\mathrm{d}}nT_{\mathrm{s}}} + \mathbf{W}(n) \tag{3}$$

where $\mathbf{W}(n)$ is the AWGN with zero mean and a defined variance. The term $\exp(\mathrm{j}2f_{\mathrm{d}}nT_{\mathrm{s}})$ models the accumulated phase change over time, where f_{d} is the frequency shift representing phase rotation applied to $\mathbf{Y}_{\mathrm{CP}}(n)$, and T_{s} is the sampling period. This accounts for Doppler effects resulting from dynamic channel behavior, which is attributed to relative motion or hardware-induced carrier frequency offsets. Removing CP yields $\mathbf{Y}(n)$, which is converted back to the frequency domain using FFT [19]:

$$\mathbf{Y}'(k) = \mathrm{FFT}\left[\mathbf{Y}(n)\right] = \left[\mathbf{H}_{\mathrm{sea}}(k)\mathbf{X}_{\mathrm{CP}}(k)\right]\mathbf{D}(k) + \mathbf{W}(k). \tag{4}$$

Here, $\mathbf{H}_{\mathrm{sea}}(k)$, $\mathbf{X}_{\mathrm{CP}}(k)$, and $\mathbf{W}(k)$ are the FFT output of $\mathbf{H}_{\mathrm{sea}}(n)$, $\mathbf{X}_{\mathrm{CP}}(n)$, and $\mathbf{W}(n)$, respectively. $\mathbf{D}(k)$ is the frequency-domain representation of $\exp(\mathrm{j}2f_{\mathrm{d}}nT_{\mathrm{s}})$, and * denotes convolution over subcarriers. After guard band removal, the frequency-domain signal is input to the LSTM network for DL-based demodulation. All OFDM symbols across all subcarriers at time t are fed to an LSTM network that demodulates the b^{th} subcarrier. For each data subcarrier b, the LSTM network processes input X_t across T time steps to output $y_{b,t}$ as the demodulated output of the b^{th} data subcarrier at time t. This demodulation process is conducted at each OFDM data subcarrier, and the demodulated output for each data subcarriers are then concatenated to form

$$\mathbf{Y}_t = \left[y_{1,t'}, y_{2,t'}, \ldots, y_{B,t'}\right] \tag{5}$$

where the full demodulated OFDM symbols over time T are

$$\mathbf{Y}_{\varsigma} = \left[\mathbf{Y}_1, \mathbf{Y}_2, \ldots, \mathbf{Y}_T\right] \in \mathbb{C}^{T\times B}. \tag{6}$$

2.3 The Undersea RF Channel under Consideration

This section describes the two representative cases of undersea RF transmission that are considered. As depicted in Fig. 1, Case 1 considers transmission between sensors and a data relay unit, which is primarily a direct wave between the transmitting and receiving antennas. This scenario is modeled as a line of sight (LOS) transmission between a pair of transmitting and receiving antennas separated by a distance d. Here, the antenna height h is assumed to be sufficiently large. Hence, only a direct wave along Path 1 exists in the channel (Fig. 5(a)). The channel, therefore, emulates a LOS channel with AWGN. The path loss L_{sea} for Case 1 is defined by [19] as

$$L_{\mathrm{sea}} = L_{\mathrm{Path1}} = 10\log_{10}\left(\mathrm{e}^{-2\alpha d}\right) \tag{7}$$

where d is the distance between the transmitting and receiving antennas, and α is the attenuation constant given by [21] as

$$\alpha = \omega\sqrt{\frac{\mu\varepsilon}{2}\left(\sqrt{1+\left(\frac{\sigma}{\omega\varepsilon}\right)^2}-1\right)}. \tag{8}$$

Here, $\omega = 2\pi f_{\mathrm{c}}$ $\omega = 2\pi f_c$ and ε, μ, and σ are the permittivity, permeability, and conductivity of sea water.

Conversely, Case 2 considers RF signal transmission between sensors placed near the seabed. In this scenario, the antenna height h is assumed to be sufficiently small, inducing a lateral wave along the seabed [22–24]. Figure 5(b) illustrates a case modeled by both the direct wave along Path 1 and lateral waves propagating along Path 2. This channel is modeled as a two-ray Rician fading channel, where the direct wave corresponds to the dominant LOS path, and the lateral wave represents multipath caused by the near-seabed propagation. For simplicity, a quasi-static fading channel is assumed, given the low-mobility nature of the environment. The channel incorporates physical layer propagation effects such as attenuation constants, boundary loss at the seawater-seabed interface, and differential delay between the two paths. We define the total path loss L_{seabed} as

$$\begin{aligned}L_{\mathrm{seabed}} &= L_{\mathrm{Path\,2}} + 2L_{\mathrm{Path\,1}} + L_{\mathrm{boundary}} = \\ &10\log_{10}\left(\mathrm{e}^{-2\alpha_{\mathrm{sb}}d_{\mathrm{sb}}}\right) + 2\left[10\log_{10}\left(\mathrm{e}^{-2\alpha d}\right)\right] + L_{\mathrm{boundary}}\end{aligned} \tag{9}$$

where the attenuation constant for the lateral wave α_{sb} is derived from [21] as

$$\alpha_{\mathrm{sb}} = \omega \sqrt{\frac{\mu_{\mathrm{sb}}\varepsilon_{\mathrm{sb}}}{2}\left(\sqrt{1+\left(\frac{\sigma_{\mathrm{sb}}}{\omega\varepsilon_{\mathrm{sb}}}\right)^2}-1\right)} \tag{10}$$

and ε_{sb}, μ_{sb}, and σ_{sb} are the permittivity, permeability and conductivity of the seabed. The boundary loss L_{boundary} is defined by [21] as

$$L_{\mathrm{boundary}} = \left|\frac{Z_2 - Z_1}{Z_2 + Z_1}\right| \tag{11}$$

where Z_1 and Z_2 are the intrinsic impedance of seawater and the seabed, respectively. The intrinsic Z for a medium is given by [21]

$$Z = \sqrt{\frac{\mathrm{j}\omega\mu}{\sigma + \mathrm{j}\omega\varepsilon}} \tag{12}$$

where ε and μ refer to the permittivity and permeability of the respective media. The path delay is estimated from the difference of the time-of-arrival between the direct and lateral waves, which is derived as

$$\tau = \frac{\Delta d}{c'}. \tag{13}$$

Here, Δd is the difference of path length between the direct and lateral waves' path, and c' is the effective velocity of wave, given by

$$c' = f_{\mathrm{c}}\lambda' \tag{14}$$

where the effective wavelength λ' is defined as

$$\lambda' = \frac{\lambda_0}{\sqrt{\mu_{\mathrm{r}}\varepsilon_{\mathrm{r}}}}. \tag{15}$$

Here, λ_0 is the wavelength in the atmosphere, and ε_r and μ_r are the relative permittivity and permeability of the medium, respectively. The Rician K-factor is calculated based on the ratio of received power in the direct path to that in the lateral path. The received power levels for both components were calculated using the distance-related path loss from (7) to (12).

Table 4 shows the numerically estimated undersea RF channel parameters while varying the distance between the antennas, using the system parameters, and undersea properties listed in Tabs. 2 and 3. It can be observed in the table that when the distance is 5 meters or more, the K-factor becomes significantly high, resulting in a near AWGN case for the channels, and channel equalization is not required in such cases. Therefore, in this study, we focus the performance analysis on Case 1 and Case 2 for d = 3 m, where K = 5.9. For these Rician fading cases, the multipath channel is modeled with two taps, corresponding to a dominant direct path and a weaker delayed component caused by lateral wave propagation near the seabed. The relative path delays are set to 0 and 0.5 µs, with average path gains of 0 dB and –5.9 dB, respectively. A Rician K-factor of 5.9 dB is used to characterize the power ratio between the direct and scattered paths. The system sampling rate is 2 MHz, ensuring that the delay spread remains well within the cyclic prefix duration of the OFDM symbols.

Additionally, to emulate dynamic channel conditions and hardware-induced impairments, we incorporated Doppler-induced frequency shifts into the transmitted signal. Specifically, based on (2), the time-domain baseband signal was multiplied by a complex exponential $\exp(-\mathrm{j}2f_{\mathrm{d}}nT_{\mathrm{S}})$. Two representative Doppler values were used: 10 Hz, corresponding to typical relative velocities (3–5 m/s) in underwater mobile scenarios, such as divers or AUVs [25], and 400 Hz, representing typical hardware-induced carrier frequency offsets (CFOs) commonly caused by oscillator mismatch in practical transceivers [26]. We evaluated both conventional and deep learning-based demodulators with and without CFO compensation.

2.4 Proposed LSTM Network and Training Specification

As mentioned in the previous sections, the LSTM network is implemented to process the received OFDM symbols that passed through the undersea RF channels and predict the demodulated output at the b^{th} data subcarrier. In this study, the LSTM network architecture used at each subcarrier generally follows the structure illustrated in Fig. 6. The overall network consists of an input sequence layer which receives the real and imaginary components of the received OFDM symbols, LSTM layers which are customized for each case of modulation order, fully connected layer that maps the output to their designated classes, and finally the softmax layer and output classification layer for the computation of the class probabilities and selects the most likely demodulated OFDM symbol. As shown in Fig. 6, for BPSK modulation, a network with two LSTM layers, each with 32 and 16 hidden units, was used, respectively (hereafter referred to as LSTM-Net 1). For the QPSK and 8PSK modulation schemes, three LSTM layers were employed, each with 64, 32, and 16 hidden units, respectively. This three-layer LSTM network is trained separately for QPSK (named LSTM-Net 2) and 8-PSK (named LSTM-Net 3). This modulation-based customization was implemented to optimize performance and prevent issues of underfitting and overfitting.

The LSTM networks are trained using a supervised learning approach to map received OFDM symbols to their corresponding transmitted symbols, as an M-class classifier, where M refers to the modulation order of the OFDM symbol, representing BPSK, QPSK, and 8-PSK, where the symbols are mapped to 2, 4, and 8 classes, respectively. The network is trained using the standard cross-entropy loss function [23], defined as:

$$L_{\mathrm{entropy}} = \sum_{c=1}^{C} y_c \log\left(\hat{y}_c\right) \tag{16}$$

where C is the number of symbol classes, y_{c} is the ground truth label (one-hot encoded), and $\hat{y}_c$ is the predicted probability from the softmax layer. The training process follows these steps:

1. Forward Propagation: Input sequences are fed into the LSTM network, and the predicted class probabilities are computed using the softmax activation function.
2. Loss Computation: The cross-entropy loss is calculated to measure the discrepancy between the predicted and actual symbol classes.
3. Gradient Computation & Backpropagation: Gradients are computed using the backpropagation algorithm, adjusting weights via the chosen optimizer.
4. Weight Update: Parameters are updated iteratively using mini-batch training

The size of the input sequences was $B \times$ no. of OFDM symbols. For each symbol constellation, 5000 OFDM symbols were simulated. The main hyperparameters used for training the network are summarized in Tab. 5. For each network, training was conducted under various simulated conditions, including RF undersea channels (AWGN, Rician fading channel, dynamic channel with Doppler shifts), different Eb/No levels, and varying CP length, as listed in Tab. 6.

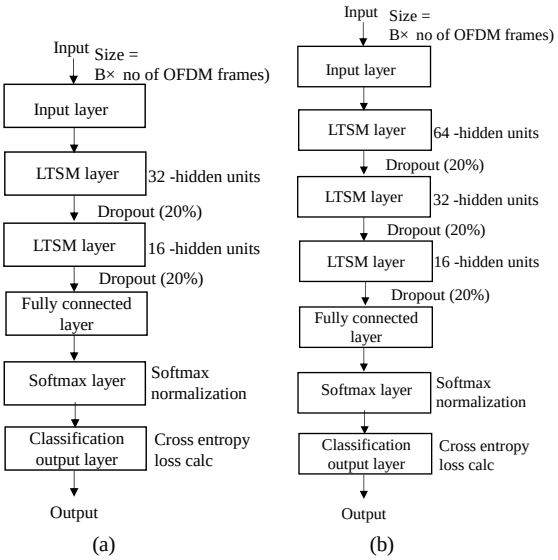

Fig. 6. Structure of the modeled LSTM network used in this study: (a) LSTM-Net 1 and (b) LSTM-Net 2 and LSTM-Net 3.

Layer	**Permittivity** ε	**Permeability** μ	**Conductivity** σ [S/m]
Seawater	$71.4\varepsilon_0$	μ_0	5.1
Seabed	$5.0\varepsilon_0$	μ_0	2.0

Tab. 3. Properties of undersea and seabed layers used in numerical calculation of undersea RF channel (Reproduced from [23]).

Parameters	**Distance, *d***			
	3 [m]	**5 [m]**	**7 [m]**	**10 [m]**
K-factor	5.9	17.2	28.5	45.5
Path delay	100 [ns]	150 [ns]	200 [ns]	250 [ns]

Tab. 4. Calculated Rician K-factor and path delay for the considered undersea RF channel (f_c = 1 MHz). The K-factor corresponding to d = 3 m (K = 5.9) was used in simulation evaluations.

Network	**Initial learning rate**	**Learn. Drop Factor**	**Minibatch size**	**Max epoch**	**Optimizer**
LSTM-Net 1	0.001	0.1	400	15	Adam
LSTM-Net 2			500	20	
LSTM-Net 3			1000	20	

Tab. 5. Hyperparameters used for training of each LSTM network used in this study.

Network	**Mod**	**Channel**	**Eb/No**	**CP Length**
LSTM-Net 1	BPSK	AWGN, Rician, Dynamic channel	2 dB, 6 dB	2, 16 [(1)]
LSTM-Net 2	QPSK		2 dB, 6 dB, 10 dB	
LSTM-Net 3	8-PSK		2 dB, 6 dB, 10 dB	

[(1)] CP = 2 and 16 correspond to 1/32 and 1/4 of the useful OFDM symbol duration, respectively.

Tab. 6. Parameters of input sequence to each LSTM network.

2.5 Hardware and Software Configuration

All simulations, including the modelling of undersea RF propagation, channel generation, and BER analysis in this study, were carried out using MATLAB R2022b on a standard desktop PC with an Intel Core i5 12500H 2.75 GHz processor, 16 GB RAM, NVIDIA GeForce RTX 3050 GPU, and Windows 11 operating system. The proposed deep learning architectures (LSTM networks) and training tasks were implemented using MATLAB's Deep Learning Toolbox.

3. Results and Discussions

3.1 Results of DL Network Training

The training and validation accuracies and losses for both networks at all of the OFDM data subcarriers are shown

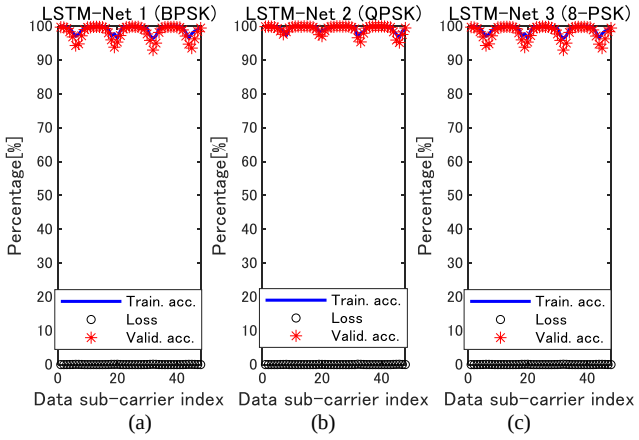

Fig. 7. Result of training accuracies, losses, and validation accuracies for the proposed networks: (a) LSTM Net 1, (b) LSTM-Net 2 for QPSK, (c) LSTM-Net 3 for 8-PSK.

in Fig. 7. It is observed from the figure that all networks achieved average training accuracy above 97%, with training losses below 0.01%, at all data subcarriers. The validation accuracy also agrees well with the training accuracies, indicating that utilization of two LSTM layers for BPSK, and three layers for QPSK and 8-PSK, is appropriate for sufficient training with no overfitting issues.

Figure 8 depicts examples of the confusion matrix obtained on the validation data set at the data subcarrier index $b = 24$, for all networks. Each confusion matrix provides a detailed breakdown of classification performance: the rows indicate the predicted classes, and the columns indicate the true transmitted classes. Diagonal cells show the number and percentage of correctly classified OFDM symbols, while off-diagonal cells correspond to misclassified symbols. The grey summary bars on the far right of each matrix visualize the precision (positive predictive value) and false discovery rate for each predicted class. Similarly, the summary bars at the bottom of the matrices represent the recall (true positive rate) and false negative rate for each true class.

The bottom-right cell shows the overall classification accuracy achieved by the network. From the figure, it can be observed that all networks demonstrated high symbol decoding and classification rates, with ground truth and predicted class matching well, except for a few small missing classes.

3.2 Performance Analysis

The performance of the proposed scheme is analyzed in terms of average bit-error-rate (BER) and benchmarked with a conventional OFDM scheme implementing channel estimation and equalization based on the LS method. The LS method is selected due to its computational simplicity and widespread use in practical OFDM systems, making it a suitable reference for assessing the potential improvements introduced by the proposed approach.

First, the BER performance is analyzed for Case 1, where the channel is equivalent to an AWGN channel (Fig. 9). The theoretical BER curves for BPSK/QPSK and 8-PSK are presented as reference. Both the simulated conventional OFDM demodulation (channel equalization is not required) and the proposed DL-based scheme produced BER curves that agreed well with the theoretical AWGN curve. Similar results were obtained for BPSK, QPSK, and 8-PSK modulation schemes, demonstrating the capability of the DL-based method to perform demodulation with comparable performance to conventional OFDM demodulation, even for higher-order modulation schemes such as 8-PSK, provided the network is properly trained. It is also worth noting that for all modulation orders, training the networks at 6 dB of E_b/N_0 is sufficient for demodulation for the whole range of 2 to 14 dB of E_b/N_0.

Next, the BER performance for Case 2, where the RF undersea channel resembles a Rician fading channel with $K = 5.9$, is analyzed. For this case, channel estimation and equalization using the LS method were applied in conventional OFDM demodulation. Figure 10(a) shows the BER performance for the case of BPSK. Conventional OFDM demodulation without channel equalization marked a BER

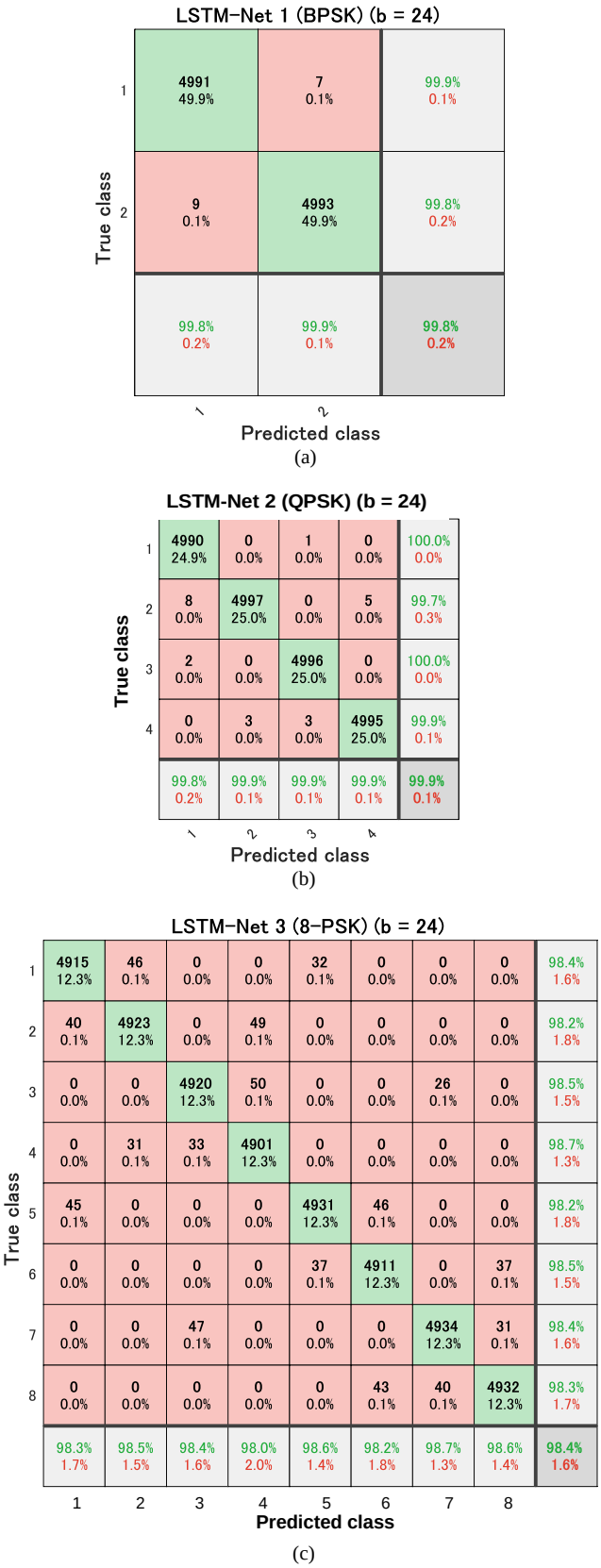

Fig. 8. Examples of confusion matrices for the proposed networks: (a) LSTM Net 1, (b) LSTM-Net 2 for QPSK, (c) LSTM-Net 3 for 8-PSK.

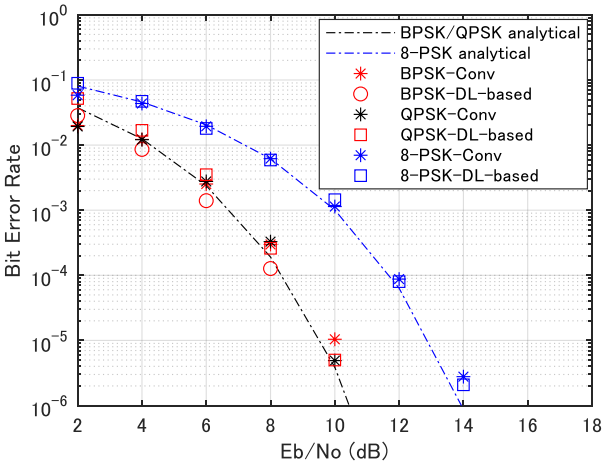

Fig. 9. BER performance of the proposed networks for Case 1 (Static AWGN channel).

floor around 0.5 across all E_b/N_0, indicating that equalization is essential for the simulated channel conditions. The LS-based equalization methods, particularly with CP = 16 (≈ 1/4 symbol duration), yield a BER curve with a similar trend to the theoretical BPSK BER curve, with approximately 2 to 4 dB degradation, but still provide reasonable performance. When the CP is shortened to 2 (≈ 1/32 symbol duration), the BER deteriorates further, indicating that inter-symbol interference (ISI) plays a vital role in performance degradation. Deep learning-based equalization notably improves the BER, demonstrating its effectiveness in handling complex channel distortions. In this scenario, the DL-based approach provides approximately 2 dB improvement over the LS-based methods. For the case of the DL-based approach, an identical BER curve was obtained with a shorter CP length (CP = 2).

The BER performance is further analyzed using higher modulation orders, namely QPSK and 8-PSK schemes. Firstly, as shown in Fig. 10(b), conventional OFDM demodulation with QPSK yields a similar BER trend to the BPSK case, either without or with equalizations, but with slight degradation. This is attributable to the reduced Euclidean distance between the QPSK symbols, compared to BPSK. Similar to the case of BPSK, reducing the CP length to 2 in the conventional QPSK demodulation degrades the BER performance. When the proposed DL-based approach is used, a significant improvement in BER was observed, providing approximately 4 dB of improvement. This implies that DL models can better capture and compensate for complex distortions in QPSK, leading to a larger performance gain compared to only 2 dB in the BPSK case.

The BER for the case of 8-PSK is observed. Figure 10(c) shows that for these simulated channel conditions, the conventional 8-PSK with the LS method has the worst BER performance compared to the other two modulation schemes, due to its much smaller Euclidean distance. From the figure, the proposed DL-based scheme provides greater BER improvements compared to the previous cases, more than 6 dB when E_b/N_0 is above 12 dB. This aligns with the expectation that deep learning-based methods, which can learn complex nonlinear channel behaviors, have a greater

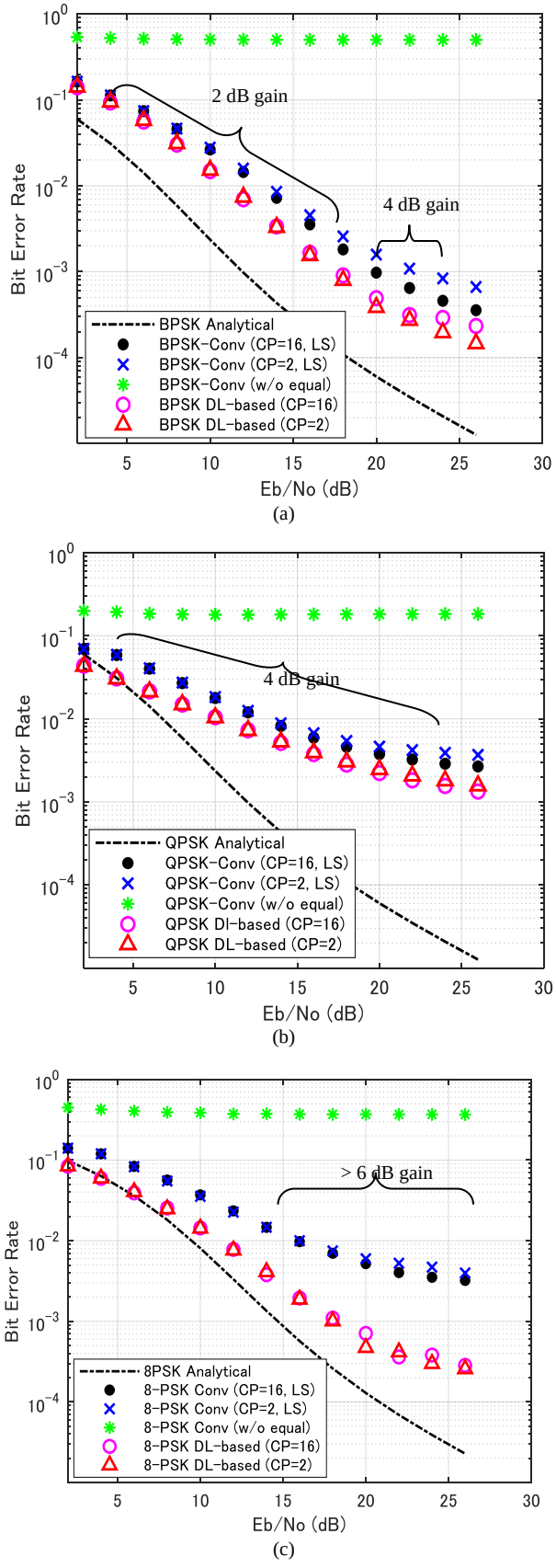

Fig. 10. BER performance of the proposed networks for Case 2 (Rician $K = 5.9$, static channel) with cyclic-prefix lengths of 2 and 16 samples (≈ 1/32, 1/4 of the useful symbol duration): (a) LSTM Net 1 (BPSK), (b) LSTM-Net 2 (QPSK), (c) LSTM-Net 3 (8-PSK).

Label	True Positive (TP)	False Positive (FP)	False Negative (FN)	Precision	Recall	F1
1	23967	23	56	0.9990	0.9977	0.9984
2	23954	56	23	0.9977	0.9990	0.9984

(a)

Label	True Positive (TP)	False Positive (FP)	False Negative (FN)	Precision	Recall	F1
1	12049	19	41	0.9984	0.9966	0.9975
2	12102	63	12	0.9948	0.9990	0.9969
3	11878	16	49	0.9987	0.9959	0.9972
4	11831	42	38	0.9965	0.9968	0.9966

(b)

Label	True Positive (TP)	False Positive (FP)	False Negative (FN)	Precision	Recall	F1
1	5988	0	3	1	0.9995	0.9998
2	6044	1	0	0.9998	1	0.9992
3	5792	4	2	0.9993	0.9996	0.9995
4	6141	2	1	0.9996	0.9998	0.9998
5	6041	3	18	0.9995	0.9970	0.9983
6	6020	18	1	0.9970	0.9998	0.9984
7	5946	12	4	0.9979	0.9993	0.9987
8	5987	1	12	0.9998	0.9980	0.9998

(c)

Tab. 7. Calculation of F1 score (E_b/N_0 = 20 dB, No. of OFDM symbols = 1000): (a) LSTM-Net 1, (b) LSTM-Net 2, and (c) LSTM-Net 3.

impact when traditional estimation techniques struggle. The classification performance in terms of F1 results for all LSTM-Net 1, LSTM-Net 2, and LSTM-Net 3 is listed in Tab. 7, calculated using 1000 OFDM symbols at E_b/N_0 = 20 dB. All networks showed excellent and consistent performance across all classes, and low error rates (False Positives/False Negatives) across the board, which suggests that the model is robust and highly accurate.

Additionally, we investigated the performance of the proposed scheme in dynamic channel conditions by observing the impact of the Doppler-induced carrier frequency offset (CFO) on demodulation accuracy by introducing uncorrected Doppler shifts at the transmitter. As shown in Fig. 11, the conventional demodulators (BPSK, QPSK, 8-PSK) exhibited severe performance degradation in the absence of CFO compensation. For example, a modest Doppler shift of 10 Hz resulted in the BER for BPSK and QPSK approaching 0.5, indicating total symbol misdetection. By contrast, our proposed DL-based demodulator, when trained with Doppler-augmented data, maintained reliable detection across all modulation formats. The performance degradation due to 10 Hz and 400 Hz Doppler was limited to approximately 1–2 dB of E_b/N_0, demonstrating strong resilience to frequency offsets. These results confirm the advantage of data-driven models in handling dynamic channel variations comprising the uncorrected Doppler shifts, subject to the inclusion of Doppler-impaired inputs in the training data.

Overall, the results indicate that the application of deep learning in place of equalization provides noticeable improvements, particularly in the simulated undersea RF channels and base OFDM system under consideration. While

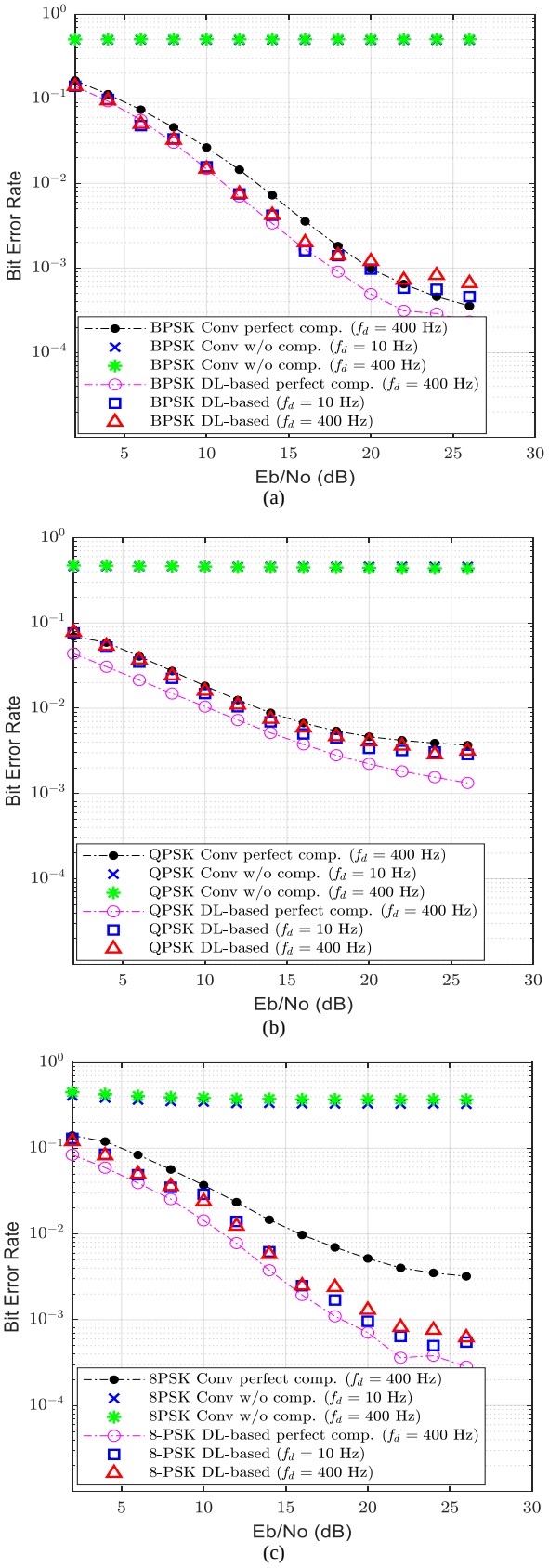

Fig. 11. BER performance of the proposed networks in dynamic channels (f_d = 10 and 400 Hz, Rician K = 5.9, CP = 16 samples (≈ 1/4 of the useful symbol duration)): (a) LSTM Net 1, (b) LSTM-Net 2 for QPSK, (c) LSTM-Net 3 for 8-PSK.

BPSK exhibits better inherent robustness due to its simpler constellation, QPSK and 8-PSK provide more data throughput, given by the additional symbols transmitted simultaneously. The improved BER from the conventional LS method in QPSK and 8-PSK suggests that the true advantage of DL-based equalization becomes more evident as modulation complexity increases. Similar traits were also reported in works such as [6], [13]. It was also observed that the proposed DL-based scheme is robust in dynamic channel conditions involving Doppler shifts.

3.3 Performance and Complexity Benchmarking

3.3.1 Performance Comparison

The proposed LSTM-based demodulator is benchmarked against existing DL-based OFDM demodulation schemes in terms of BER performance. Although originally designed for different applications and channel conditions, a 1D-CNN-based network [15] and a hybrid CNN-biLSTM-based network for 5G systems [16] are considered here, as both employ OFDM QPSK modulation and benchmark against LS methods. It should be noted that these comparisons are qualitative rather than direct, since [15] assumes a high-mobility terrestrial channel (50 km/h) and [16] reports symbol error rate (SER) under a distinct propagation environment. In contrast, our evaluation focuses on static undersea RF channels with BER as the performance metric. According to [15] and [16], the 1D-CNN and hybrid CNN-biLSTM architectures achieve BER improvements of approximately 2 dB and 4 dB compared to LS equalization, respectively. The proposed LSTM-Net 2 achieves comparable or superior gains, with 4–6 dB improvement over LS, thereby outperforming the 1D-CNN and matching or exceeding the hybrid CNN-biLSTM.

In addition, a ResNet-based demodulator we trained and evaluated under the same dataset and undersea channel conditions as LSTM-Net 2. As shown in Fig. 12, the ResNet model achieves performance broadly comparable to the proposed LSTM-based network. However, LSTM-Net 2 demonstrates slightly better BER in the low-SNR regime (2–6 dB), which is critical for reliable undersea RF communication. At higher E_b/N_0 values (above 10 dB), both the LSTM and ResNet models converge to nearly identical BER performance.

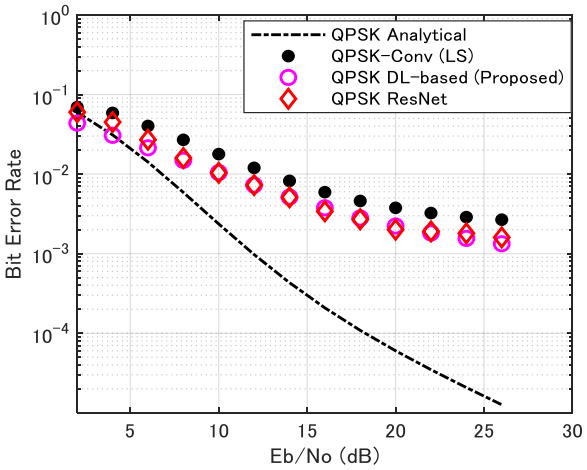

Fig. 12. BER performance comparison between the proposed LSTM-Net 2 and the ResNet-like network.

3.3.2 Computational Complexity Comparison

The computational complexity of the proposed DL-based and traditional OFDM receivers can be assessed in terms of asymptotic O notation, expanded into FLOP counts, and finally translated into inference latency on an embedded platform. The conventional OFDM receiver consists of CP removal, FFT, LS channel estimation, and ZF equalization, with a total complexity of $O(N_{\text{FFT}}\log N_{\text{FFT}} + B)$, where N_{FFT} is the FFT size and B the number of data subcarriers. Expanding this into FLOPs yields approximately $10N_{\text{FFT}}\log_2 N_{\text{FFT}}$ operations for the FFT and about $30B$ FLOPs each for LS estimation and ZF equalization. For $N_{\text{FFT}} = 64$ and $B = 48$, the total cost is approximately 5.3×10^3 FLOPs per OFDM symbol, which is computationally trivial but yields poor BER performance under the simulated Rician fading condition.

On the other hand, the computational complexity of proposed LSTM-based demodulator with h hidden units at each layer, input dimension M, and L stacked layers is $O(L(h^2 + Mh))$. In FLOPs, this corresponds to approximately $8(h^2 + Mh + h)$ operations per time step, per layer [27], [28]. Considering B number of data subcarriers and time steps T, the overall complexity scales as $\text{FLOPs}_{\text{LSTM}} \approx BTL \cdot 8(h^2 + Mh + h)$. Using the QPSK case parameters (three LSTM layers with 64, 32 and 16 hidden units), the resulting cost is approximately 3.14×10^6 FLOPs per OFDM symbol.

Other DL-based schemes follow similar derivations.

Scheme	Complexity (O-notation)	FLOPs per OFDM symbol	Parameters	Model size (FP16)	Estimated t_{proc}, $P \in [16,64]$
Conventional (LS with ZF equalization)	$O(N_{\text{FFT}}\log N_{\text{FFT}} + B)$	~ 5.3×10^3	N/A	N/A	~ 1 µs
1D-CNN [15]	$O(LFk_sN)$	~ 6.8×10^4	~ 12×10^3	~ 25 MB	~ 1 to 4 µs
CNN-biLSTM [16]	$O(\underline{LF}k_sN) + O(L(8Mh + 8h^2))$	~ 2.0×10^5	~ 85×10^3	~ 1.7 MB	~ 3 to 12 µs
ResNet	$O(2DFk_sN)$	~ 6.0×10^5	~220×10^3	~ 4.5 MB	~ 9 to 28 µs
LSTM (proposed)	$O(L(h^2 + Mh)$	~ 3.14×10^6	~25×10^3	~ 0.5 MB	~ 10 to 25 µs

Tab. 8. Computational complexity of conventional and DL-based OFDM demodulators expressed in O-notation, expanded into FLOPs per OFDM symbol, parameter count to storage size, and estimated processing latency under parallel execution ($P \in [16,64]$).

The 1D-CNN complexity is $O(LFk_sN)$, where F, k_s, and N denote the number of filters, kernel size, and input length, respectively. The CNN-biLSTM combines CNN layers with bidirectional LSTMs, doubling the recurrent cost: $O(\underline{LF}k_sN) + O(L(8Mh + 8h^2))$. The ResNet-based model, consisting of D residual blocks with two convolutional layers each, has complexity $O(2DFk_sN)$. These asymptotic expressions are expanded into FLOPs using standard layer-wise operation counts, showing that CNN-only models are most efficient, while ResNet incurs the heaviest cost due to its deep stacked convolutional blocks, as shown in Tab. 8.

To analyze the real time processing capability, the above complexity analysis must be viewed in relation to the OFDM symbol duration. With a sampling rate of 2 MHz and $N_{FFT} = 64$, the OFDM symbol duration is approximately $T_{sym} \approx 31.6$ µs. With CP lengths of 2 and 16 samples (equivalent to 1/32 and 1/4 of the useful symbol duration, respectively), the extended durations become roughly 32.6 µs and 39.6 µs, respectively. These values define the hard processing deadline per symbol. Since the proposed LSTM-based demodulator requires about 3.1×10^6 FLOPs per OFDM symbol, its latency must remain below this deadline to ensure real-time operation. Let C_{sym} be the computation time per OFDM symbol (in FLOPs) and $\emptyset$ the effective sustained throughput of the processor (in FLOPs/s). With P parallel workers (e.g., SIMD lanes, NPU tiles, CUDA warps, or FPGA processing elements), the amortized per-symbol latency is

$$t_{proc} \approx \frac{C_{sym}}{\emptyset \cdot P}. \tag{17}$$

Given with modest effective throughputs in the multi-GFLOP/s class and parallelism levels $P \in [16, 64]$ [29], the amortized per-symbol latency of the proposed DL-based demodulation typically falls in the range of 10–25 µs, depending on hardware throughput and degree of parallelism. Both ranges are well below the deadline dictated by the symbol duration. In practice, batching and pipelined execution across OFDM symbols further improve throughput, while model-level optimizations (e.g., INT8/FP8 quantization, pruning, kernel fusion) reduce C_{sym}. Hence, the proposed demodulator is well matched to parallelism-based processors (mobile NPUs, embedded GPUs, FPGAs, or DSPs with wide SIMD), meeting real-time constraints without reliance on a single specific device.

For completeness, we also discuss the model size in terms of trainable parameters. Parameter counts can be generalized for each architecture using their dominant scaling terms. Specifically, the LSTM network scales as $O(h^2 + Mh)$, CNN layers as $O(Fk_sM)$, CNN-biLSTM as a combination of CNN and bidirectional LSTM ($O(Fk_sM + h^2 + \underline{M}h)$), and ResNet blocks as $O(DFk_sM)$. Here, M the input dimension. For the proposed three-layer LSTM network (64–32–16 hidden units, QPSK case), this results in approximately 25k parameters, corresponding to < 0.5 MB of model size in FP16 (16-bit floating point) precision, a widely adopted low-precision format in embedded AI accelerators. This is significantly smaller than ResNet-like architectures (≈ 220k parameters with ≈ 4.5 MB model size), ensuring that storage and memory overheads remain modest for deployment on embedded devices (Tab. 8).

In summary, the complexity and latency analyses confirm that the proposed LSTM-based demodulator achieves a balanced trade-off between computational demand and BER performance. While more demanding than lightweight CNN-only models, it remains significantly less complex than deeper ResNet-style architectures and is capable of meeting hard real-time deadlines dictated by the OFDM symbol duration. The analysis further shows that, with modest levels of parallelism, the per-symbol processing time remains in the order of tens of microseconds, comfortably below the symbol interval (32–40 µs) used in our system. These results demonstrate that the proposed approach is not only effective in terms of reliability under challenging undersea RF conditions but also practical for deployment on modern embedded processors with parallelism support.

4. Concluding Remarks

This paper presented an investigation of a DL-based OFDM receiver for short-range undersea wireless communication, where an LSTM network is employed at the OFDM receiver to replace conventional channel estimation, equalization, and symbol demapping. The LSTM-based network is trained using supervised learning, with varying architectures optimized for BPSK, QPSK, and 8-PSK. By leveraging sequential feature extraction of LSTM, the proposed approach eliminates reliance on explicit channel estimation, thereby improving robustness and complexity. The LSTM network is evaluated in two representative cases of data transmission mode in an undersea wireless sensor network, where a direct wave and both the direct and lateral waves are considered. It was found that in the direct wave case, the proposed scheme performs equally with conventional demodulation. For the case of near seabed transmission, the proposed DL-based OFDM scheme marked improved BER performance compared to conventional demodulation using the LS channel equalization method, by 2 to 4 dB. This BER gain is more evident at higher modulation orders such as 8-PSK, indicating more than 6 dB of improvement. It was also observed that the proposed DL-based scheme was resilient to frequency offsets in dynamic channel conditions involving Doppler shift.

While the current results offer a strong proof-of-concept for the proposed scheme in controlled simulation environments, we acknowledge that real-world deployment may be affected by practical environmental factors that were not explicitly considered. These include hardware-induced impairments, such as analog-to-digital converter (ADC) quantization noise and oscillator phase noise, as well as dynamic channel conditions like time variation and Doppler spread due to mobility, which are evaluated in full detail.

To date, performance evaluation has been limited to AWGN and Rician fading channels, which are appropriate for capturing typical underwater RF conditions, particularly

with dominant line-of-sight and moderate multipath propagation. However, we recognize that more complex and time-varying fading behavior may occur in practice. As part of our future work, we plan to evaluate the model under time-varying fading channels using stochastic models (e.g., time-correlated Rician profiles) and assess hardware effects through hardware-in-the-loop testing on software-defined radio (SDR) platforms.

We also plan to experimentally validate the proposed demodulator on an SDR platform in a controlled laboratory. A preliminary testbed has been developed using Ettus USRP N210 devices and custom underwater antennas, with experiments conducted in a seawater-filled tank to emulate short-range undersea conditions. Initial measurements demonstrate BER improvement over conventional demodulation by approximately 4–6 dB, supporting the feasibility of real-time hardware deployment. These results have been reported in a recent published work [30] and are not reproduced here to avoid content duplication and ensure copyright compliance.

Furthermore, future work will explore the extension of the proposed model to more complex modulation schemes such as quadrature amplitude modulation (QAM) and investigate low-latency, energy-efficient deployment on embedded AI accelerators (e.g., NVIDIA Jetson and Xilinx Zynq FPGA). Successful implementation of the trained LSTM models on these platforms will enable the proposed scheme to operate as a drop-in demodulation module in SDR-based underwater wireless systems.

Acknowledgments

This work is funded by the Competitive Research Fund of The University of Aizu (P-25).

References

[1] SMOLYANINOV, I. I., BALZANO, Q., BARRY, M. Transmission of high-definition video signals and detection of the objects underwater using surface electromagnetic waves. *IEEE Journal of Oceanic Engineering*, 2024, vol. 49, no. 2, p. 566–571. DOI: 10.1109/JOE.2023.3335599

[2] MOHD ZALI, H., MAHMOOD, M. K. A., PASYA, I., et al. Narrowband and wideband EMW path loss in underwater wireless sensor network. *Sensor Review*, vol. 42, no. 1, p. 125–132. DOI: 10.1108/SR-04-2021-0128

[3] ABDOU, A. A., SHAW, A., MASON, A., et al. Electromagnetic (EM) wave propagation for the development of an underwater Wireless Sensor Network (WSN). In *Proceedings of the 2011 IEEE Sensors.* Limerick (Ireland), 2011, p. 1571–1574. DOI: 10.1109/ICSENS.2011.6127319

[4] SMOLYANINOV, I., BALZANO, Q., YOUNG, D. Development of broadband underwater radio communication for application in unmanned underwater vehicles. *Journal of Marine Science and Engineering*, 2020, vol. 8, no. 5, p. 370–380. DOI: 10.3390/jmse8050370

[5] HONKALA, M., KORPI, D., HUTTUNEN, J. M. J. DeepRx: Fully convolutional deep learning receiver. *IEEE Transactions on Wireless Communications*, 2021, vol. 20, no. 6, p. 3925–3940. DOI: 10.1109/TWC.2021.3054520

[6] KIM, J., LEE, H., HONG, S. E., et al. Deep learning methods for universal MISO beamforming. *IEEE Wireless Communications Letters*, 2020, vol. 9, no. 11, p. 1894–1898. DOI: 10.1109/LWC.2020.3007198

[7] SAFI, H., TAYAKKOLNIA, I., HAAS, H. Deep learning based end-to-end optical wireless communication systems with autoencoders. *IEEE Communications Letters*, 2024, vol. 28, no. 6, p. 1342–1346. DOI: 10.1109/LCOMM.2024.3387286

[8] JIANG, X., LIANG, K., CHU, X., et al. Multiplexing eMBB and URLLC in wireless powered communication networks: A deep reinforcement learning-based approach. *IEEE Wireless Communications Letters*, 2023, vol. 12, no. 10, p. 1716–1720. DOI: 10.1109/LWC.2023.3290040

[9] ISMAYILOV, R., CAVALCANTE, R. L. G., STAŃCZAK, S. Deep learning beam optimization in millimeter-wave communication systems. In *Proceedings of* the *2021 IEEE Statistical Signal Processing Workshop (SSP)*. Rio de Janeiro, (Brazil), 2021, p. 581–585. DOI: 10.1109/SSP49050.2021.9513817

[10] GAO, W., ZHANG, W., LIU, L., et al. Deep residual learning with attention mechanism for OFDM channel estimation. *IEEE Wireless Communications Letters*, 2025, vol. 14, no. 2, p. 250–254. DOI: 10.1109/LWC.2022.3232378

[11] LV, C., LUO, Z. C. Deep learning for channel estimation in physical layer wireless communications: Fundamental, methods, and challenges. *Electronics*, 2023, vol. 12, no. 24, p. 1–38. DOI: 10.3390/electronics12244965

[12] GIZZINI, A. K., CHAFII, M. Deep learning based channel estimation in high mobility communications using Bi-RNN networks. In *Proceedings of the 2023 IEEE International Conference on Communications*. Rome (Italy), 2023, p. 2607–2612. DOI: 10.1109/ICC45041.2023.10278783

[13] LIU, X., SONG, Y., ZHU, J., et al. An efficient deep learning model for automatic modulation classification. *Radioengineering*, 2024, vol. 33, no. 4, p. 713–720. DOI: 10.13164/re.2024.0713

[14] HASINI, D., REDDY, K. R. L. Channel estimation and signal detection in OFDM systems using deep learning. In *Proceedings of the 2023 9th International Conference on Advanced Computing and Communication Systems (ICACCS)*. Coimbatore (India), 2023, p. 1337–1340. DOI: 10.1109/ICACCS57279.2023.10112696

[15] SIRIWANITPONG, K., SANADA, K., HATANO, H., et al. Deep learning-based channel estimation with 1D CNN for OFDM systems under high-speed railway environments. *IEEE Access*, 2025, vol. 13, p. 13128–13142. DOI: 10.1109/ACCESS.2025.3531009

[16] RAHMAN, M. H., SEJAN, M. A. S., AZIZ, M. A., et al. HyDNN: A hybrid deep learning framework based multiuser uplink channel estimation and signal detection for NOMA-OFDM system. *IEEE Access*, 2023, vol. 11, p. 66742–66755. DOI: 10.1109/ACCESS.2023.3290217

[17] ZHANG, Y., CHANG, J., LIU, Y., et al. Deep learning based underwater acoustic OFDM receiver with joint channel estimation and signal detection. In *Proceedings of the 2022 IEEE International Conference on Signal Processing, Communications and Computing (ICSPCC)*. Xiamen (China), 2022, p. 1–5. DOI: 10.1109/ICSPCC55723.2022.9984340

[18] LI, Y., WANG, S., LIU, D., et al. TransDetector: A transformer-based detector for underwater acoustic differential OFDM communications. *IEEE Transactions on Wireless Communications*, 2024, vol. 23, no. 8, p. 9899–9911. DOI: 10.1109/TWC.2024.3367179

[19] PASYA, I., MEGAT ALI, M. S. A. Evaluation of a deep learning-based orthogonal frequency division multiplexing (OFDM) scheme for undersea RF communication. In *Proceedings of the 2024 IEEE Asia-Pacific Conference on Applied Electromagnetics (APACE)*. Langkawi (Malaysia), 2024, p. 47–50. DOI: 10.1109/APACE62360.2024.10877407

[20] PROAKIS, J. G., SALEHI, M. *Digital Communications*. 5th ed. New York (USA): McGraw-Hill Education, 2007. ISBN: 9780072957167

[21] BALANIS, C. A. *Balanis' Advanced Engineering Electromagnetics*. 3rd ed. New Jersey (USA): John Wiley & Sons, 2023. ISBN: 9781394180011

[22] NIE, Z., WANG, S., DENG, T., et al. Research on low-loss and high-speed seabed propagation model for underwater Radio-Frequency-Electromagnetic communication. In *Proceedings of the OCEANS 2017-Aberdeen.* Aberdeen (Scotland), 2017, p. 1–8. DOI: 10.1109/OCEANSE.2017.8084595

[23] KAWAMURA, T., MATSUSHITA, T., KANEKO, Y., et al. Experimental observation of lateral wave propagation along seabed. In *Proceedings of 2023 IEEE International Symposium on Antennas and Propagation and USNC-URSI Radio Science Meeting (USNCURSI)*. Portland (OR, USA), 2023, p. 273–274. DOI: 10.1109/USNC-URSI52151.2023.10238122

[24] NIE, Z., WANG, S., CHEN, D., et al. Seabed-rock-layer electromagnetic communication channel model with low path loss based on evanescent wave. *Radioengineering*, 2018, vol. 27, no. 2, p. 431–439. DOI: 10.13164/re.2018.0431

[25] FU, J., LI, J., SUN, S., et al. High precision velocity estimation of AUV in an underwater distributed sensor network. *IEEE Sensors Journal*, 2022, vol. 22, no. 13, p. 13212–13225. DOI: 10.1109/JSEN.2022.3177458

[26] MIHALJEVIĆ, A., LIPOVAC, A., LIPOVAC, V., et al. Practical BER-based estimation of residual OFDM CFO by reducing noise margin. *Wireless Communications and Mobile Computing*, 2020, vol. 2020, p. 1–5. DOI: 10.1155/2020/8881436

[27] SZE, V., CHEN, Y.-H., YANG, T.-J., et al. Efficient processing of deep neural networks: A tutorial and survey. *Proceedings of the IEEE*, 2017, vol. 105, no. 12, p. 2295–2329. DOI: 10.1109/JPROC.2017.2761740

[28] HE, K., ZHANG, X., REN, S., et al. Deep residual learning for image recognition. In *Proceedings of the IEEE Conference on Computer Vision and Pattern Recognition (CVPR)*. Las Vegas (NV, USA), 2016, p. 770–778. DOI: 10.1109/CVPR.2016.90

[29] SHARMA, A., HAQ, S. A. U., DARAK, S. J. Low complexity deep learning augmented wireless channel estimation for pilot-based OFDM on Zynq system on chip. *IEEE Transactions on Circuits and Systems I: Regular Papers*, 2024, vol. 71, no. 5, p. 2334–2347. DOI: 10.1109/TCSI.2024.3371780

[30] PASYA, I., MEGAT ALI, M. S. A., RAHMAN, N. H. A. Testbed development of a deep learning-based OFDM scheme for undersea RF communication over software defined radio platform. In *Proceedings of 22nd International Conference on Electrical Engineering, Computer, Telecommunication, and Information Technology (ECTI-CON)*. Bangkok (Thailand), 2025, p. 1–5. DOI: 10.1109/ECTI-CON64996.2025.11100869

About the Authors ...

Idnin PASYA received his Bachelor of Engineering, Master of Engineering, and Doctor of Engineering degrees in Information and Communication Engineering from Tokyo Denki University in 2004, 2006, and 2015, respectively. He worked as an Engineer at Toshiba PC and Network, Tokyo, Japan, from 2006 until 2009. Dr. Idnin later joined the Faculty of Electrical Engineering of Universiti Teknologi MARA, Malaysia, from 2010 until 2023. He currently serves as an Associate Professor in the Department of Computer Science and Engineering, University of Aizu, Fukushima, Japan. His research interests include deep learning based wireless communications, antennas and propagation, underwater communications, and radar systems applications.

Megat Syahirul Amin MEGAT ALI was born in Kuala Lumpur, Malaysia. He received his Ph.D. from Universiti Teknologi MARA, Malaysia. His research interests include digital signal processing and machine learning, particularly in the development of intelligent analytical systems.

Azrul Amri JAMAL is an Associate Professor at Universiti Sultan Zainal Abidin (UNISZA), Malaysia. He obtained his Ph.D. from Bangor University, Wales, UK. He received his M.Eng. in Electronics & Computing and B.Eng. Computer Engineering from Takushoku University, Tokyo, Japan. His research interests include Internet of Things, computer networks, and communication. He is currently the head of IoT, Machines, and Systems (IMachS) Special Interest Group in UNISZA.